Hindawi
International Journal of Antennas and Propagation
Volume 2017, Article ID 7983567, 9 pages
https://doi.org/10.1155/2017/7983567

Research Article

A High Selectivity, Miniaturized, Low Profile Dual-Band Bandpass FSS with a Controllable Transmission Zero

Wenxing Li and Yuanyuan Li

College of Information and Communications Engineering, Harbin Engineering University, Harbin 150001, China

Correspondence should be addressed to Yuanyuan Li; liyuanyuan008@hrbeu.edu.cn

Received 5 March 2017; Revised 27 April 2017; Accepted 4 May 2017; Published 3 July 2017

Academic Editor: Angelo Liseno

A novel, highly selective, low profile dual-band, and bandpass miniaturized-element frequency selective surface is proposed to realize stable angular responses and a controllable transmission zero. This FSS is a three-layer structure consisting of three metal layers that are separated from each other by two dielectric substrates. The equivalent circuit model of the FSS and its operating principle are presented and analyzed based on the microwave filter theory. The prototype of this FSS is simulated, fabricated, and measured, and its theoretical analysis, simulation, and measurement results show a good agreement. This FSS has achieved an excellent angular stability and wide out-of-band rejection performance in the scope of incidence angle of 80 degrees. Compared with the other multilayered FSSs and 3D FSSs proposed in previous works, it possesses a lower profile as well as a smaller size. A transmission zero is produced by etching slots on the edges of the middle metal layer to achieve superior frequency selectivity. By properly choosing the size and direction of the slots, the transmission zero and the polarization selectivity are able to be changed, respectively.

1. Introduction

Frequency selective surfaces (FSSs) are two-dimensional periodic structures that are composed of periodically arranged patches or aperture elements. They can act as spatial filters which have a selective effect on the incident angle, polarization, and frequency of EM waves [1]. Frequency selective surfaces have been employed in a wide range of applications including radar radomes [2], RCS reduction of an antenna array [3], transmission or reflection of EM waves at different frequencies as reflectors [4–6], polarization converter [7], and microwave absorber [8, 9]. With the rapid development of radars and wireless communicating technologies, there has been an increasing demand for a miniaturized dual-band frequency selective surface in modern communication systems [10]. The main methods used to design dual-band frequency selective surfaces are perturbation technique [11, 12], fractal technology [13], combination technology [14], complementary technology [15], multilayered technology [16–21], and 3D FSS [22–26]. The perturbation technique is a mean of increasing the perturbation between cells or units to convert a single band frequency selective surface into a dual-band surface. Fractal technology is utilized to realize multiband frequency resonance by the self-similarities of elements. Combination technique is to etch different patterns on one element. The complementary method is to etch complementary patterns on both sides of a dielectric substrate. These surfaces are advantageous owing to lower profile and a simpler fabrication. The high-frequency band, however, has a null modal interaction and a grating lobe with a growing incident angle. Also, its selectivity is somewhat low. Recently, multilayered FSSs and 3D FSSs have been utilized to overcome the shortcomings of single-layered FSS structures. In [22], a 3D FSS has been proposed to obtain the performance of a triband bandpass performance. The unit cell size and the thickness of the FSS are $0.1\lambda \times 0.08\lambda$ and 0.09λ. Li and Shen have proposed a 3D FSS with the unit cell size and the thickness of $0.06\lambda \times 0.045\lambda \times 0.083\lambda$ to obtain a stable dual-band bandpass performance in [23]. Though a 3D FSS exhibits fair performances, its structure is usually more complicated than that of a traditional 2D FSS. Particularly, what should be noticed is that the profile is thick. To realize highly selective FSS with wide out-of-band rejection behaviors, some multilayered FSSs have been studied. Despite the triband FSS presented in [14], the

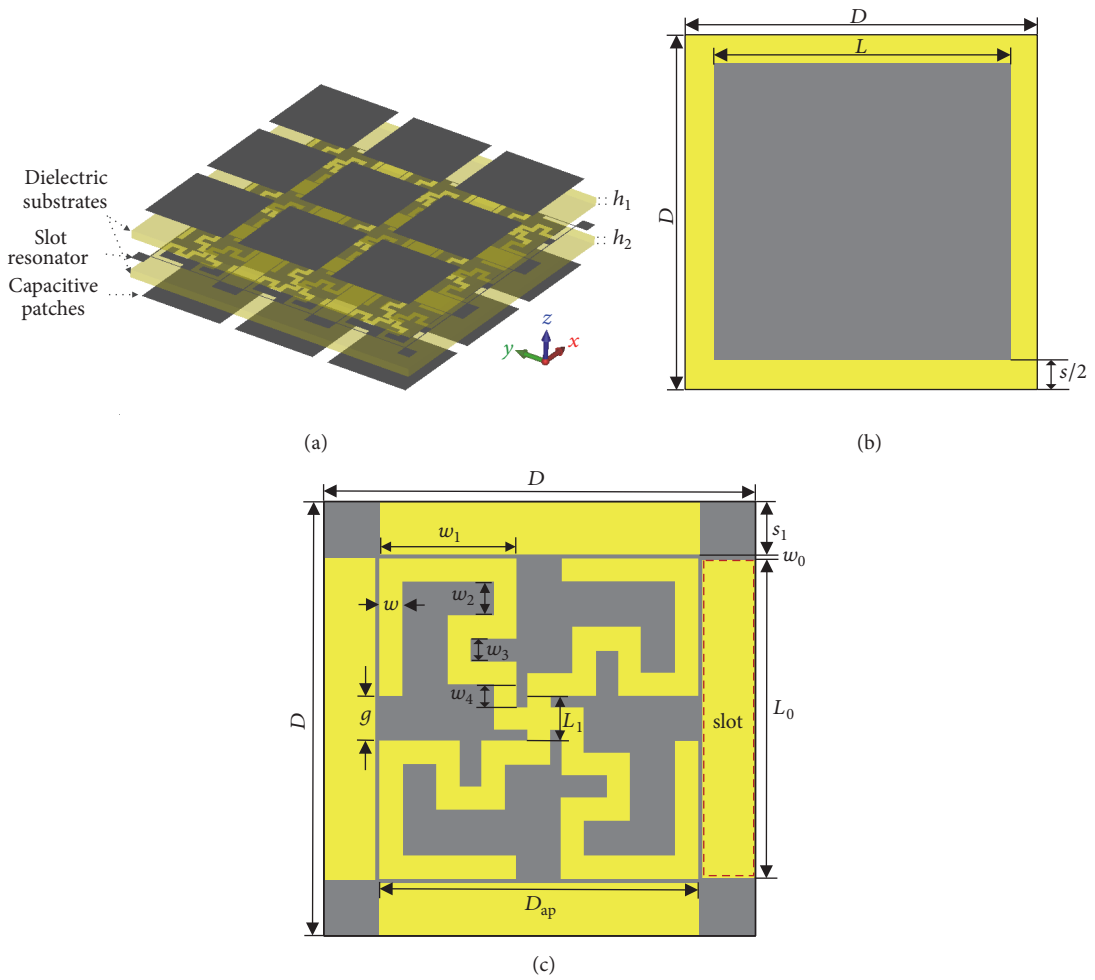

FIGURE 1: Topology of the proposed FSS. (a) The 3D view of the dual-band FSS; (b) the unit cell on the top and bottom layer; (c) the unit cell on the middle layer.

circular aperture coupled FSS in [15] and the dual-band FSS proposed by [16] have demonstrated a high selectivity and a wide out-of-band rejection. The profile is thick, and the unit size is large. In [17], a dual-band FSS with high selectivity is presented, but a modal interaction null has occurred in the high-frequency band when the incident angle increases. A dual-band FSS based on the inductance couple proposed in [19] had a satisfactory performance of selectivity and angular stability. But its insertion loss is high due to the high dielectric constant substrate.

In this paper, a dual-band bandpass miniaturized FSS with a highly selective performance and low profile is presented, which is capable of achieving a better angular stability and out-of-band rejection with the incident angle of TE and TM polarization scanning from 0 to 60 degrees. The unit cell size of the proposed design is $0.089\lambda \times 0.089\lambda$, with the overall thickness being 0.014λ, where λ is the free space wavelength of resonance frequency in the lower frequency band. A transmission zero is introduced by etching slots in the middle layer. A polarization selective surface is to be obtained by etching slots in one direction only. The operating principle, designing process, and the measurement results of the proposed FSS are presented and discussed in this paper.

2. Operating Principle and Design Procedure

2.1. Topology of FSS and Equivalent Circuit Model. Figure 1(a) shows the extended three-dimensional topology of the proposed FSS. The structure is comprised of three metal layers separated by two dielectric substrates. The unit cell is designed symmetrically in x and y directions to reduce the sensitivity of polarization and incident angle. The unit cells on the top and bottom layer are composed of square metal patches, while the unit cell on the middle layer is a resonant aperture. To produce a high selectivity FSS, a transmission zero is introduced by etching four slots in the middle layer shown in Figure 1(c).

An FSS behaves as either a series or parallel RLC circuit, depending on its filtering characteristics [18, 27]. Figure 2 shows the equivalent circuit model of the proposed FSS which provides more insight into the FSS response. In particular,

Table 1: Electrical and geometric parameters of the proposed dual-band FSS discussed in Section 2.2.

(a) Normalized quality factors and coupling coefficient for Butterworth filter response

Parameter	q_1	q_2	k_{12}	r_1	r_2
Value	1.4142	1.4142	0.70711	1	1

(b) Optimized equivalent circuit values (Figure 2)

Parameter	L_1 (pH)	L_s (pH)	C_1 (pF)	C_2 (pF)	C_3 (pF)
Value	366.2	361.7	8.03	0.29	0.29

(c) Physical dimensions of designed FSS

Parameter	D	L	L_1	L_0	g	s	s_1	w	w_0	w_1	w_2	w_3	w_4	h
Value (mm)	9.5	8	1	7	1	3	1.15	0.5	0.1	3	0.75	0.5	0.5	0.762

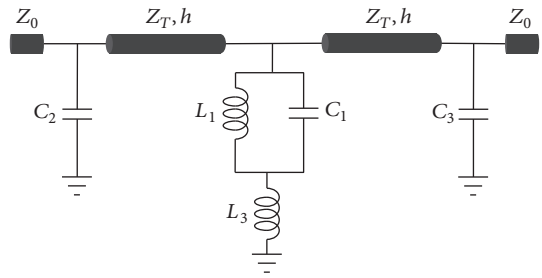

Figure 2: The equivalent circuit model of the proposed dual-band FSS.

it helps to understand the tuning mechanism of the transmission zero. The equivalent circuit model of this dual-band FSS is illustrated in Figure 2, which is valid for the incident EM wave of vertical polarization along the x direction. The patches on the top layer and on the bottom layer in the circuit model are modelled with parallel capacitors of C_2 and C_3, which are proportional to the length L of the patch and inversely proportional to the gap s between the adjacent elements, respectively. The intermediate metal layer acts in the manner of a hybrid resonator composed of L_1, C_1, and L_s as shown in the middle part of Figure 2. L_1denotes the equivalent inductance of the thin wire with the length L_0 and a width of w_0. The convoluted cross dipole aperture with the length l and width w acts as a capacitor C_1. The inductance L_s denotes the inductance of the metal patches in the corner of the middle metal layer. The dielectric substrates, sandwiched between the metal layers, are equivalent to short transmission lines. Its impedance is $Z_T = Z_0/\sqrt{\varepsilon_r}$, where $Z_0 = 377\,\Omega$ is the wave impedance in free space and ε_r is the relative permittivity of the dielectric substrate.

It is evident that when the hybrid resonator resonates, a transmission zero and a transmission pole are produced at the resonant frequencies f_{z1} and f_{01}. The capacitances C_2 and C_3 and the inductance L_s produce a resonant frequency f_{02} by coupling with the dielectric substrates.

To better illustrate the working principle of the dual-band FSS, the circuit in Figure 2 is divided into two parts. One part is the hybrid resonator which determines the low-frequency passband, and the other part which determines the high-frequency passband is shown in Figure 3(a).

The equivalent circuit in Figure 3(a) is simplified to the circuit shown in Figure 3(b), the transmission lines in which are replaced with their equivalent circuit model composed of a series inductor and a shunt capacitor. This circuit is a second-order coupled-resonator bandpass filter. A classic second-order coupled-resonator bandpass filter can be achieved by converting the T-network composed of inductors L_{T1}, L_{T2}, and L_s in Figure 3(b) to a π-network composed of inductors L_2, L_m, and L_3 as shown in Figure 3(c) [28].

The resonant frequencies are expressed as

$$f_{01} = \frac{1}{2\pi}\sqrt{L_1 C_1},$$
$$f_{z1} = \frac{1}{2\pi}\sqrt{\frac{L_1 + L_s}{L_1 L_s C_1}}. \tag{1}$$

2.2. Design Procedure of the Proposed Dual-Band FSS. The design process of the FSS is based on the circuit model in Figures 2 and 3 to synthesize the desired filter response and then calculate the geometric parameters from the parameters of the circuit. The equivalent circuit in Figure 3 is analyzed and calculated by the method presented in [29]. The center frequency of the high-frequency passband f_{02} and the value of the fractional bandwidth have been specified first, δ, and then all the equivalent parameters in Figure 2 are determined. What follows is the detailed design process.

Inductors L_{T1}, L_{T2}, and L_s in Figure 3(b) can be calculated by the following equations:

$$L_{T1} = \frac{Z_0 r_1}{w_0 q_1 k_{12}} \times \frac{k_{12}\delta}{1-(k_{12}\delta)^2} \times \left(1 - k_{12}\delta\sqrt{\frac{q_1}{q_2}\frac{r_2}{r_1}}\right),$$
$$L_{T2} = \frac{Z_0 r_2}{w_0 q_2 k_{12}} \times \frac{k_{12}\delta}{1-(k_{12}\delta)^2} \times \left(1 - k_{12}\delta\sqrt{\frac{q_2}{q_1}\frac{r_1}{r_2}}\right), \tag{2}$$
$$L_s = \frac{Z_0}{w_0 k_{12}} \times \frac{(k_{12}\delta)^2}{1-(k_{12}\delta)^2} \times \left(1 - k_{12}\delta\sqrt{\frac{r_1}{q_1}\frac{r_2}{q_2}}\right),$$

where r_1 and r_2 are normalized source and load impedance, q_1 and q_2 are normalized loaded quality factors of the resonators, and k_{12} is the coupling coefficient between the two resonators. All these parameters listed in Table 1 are determined by the

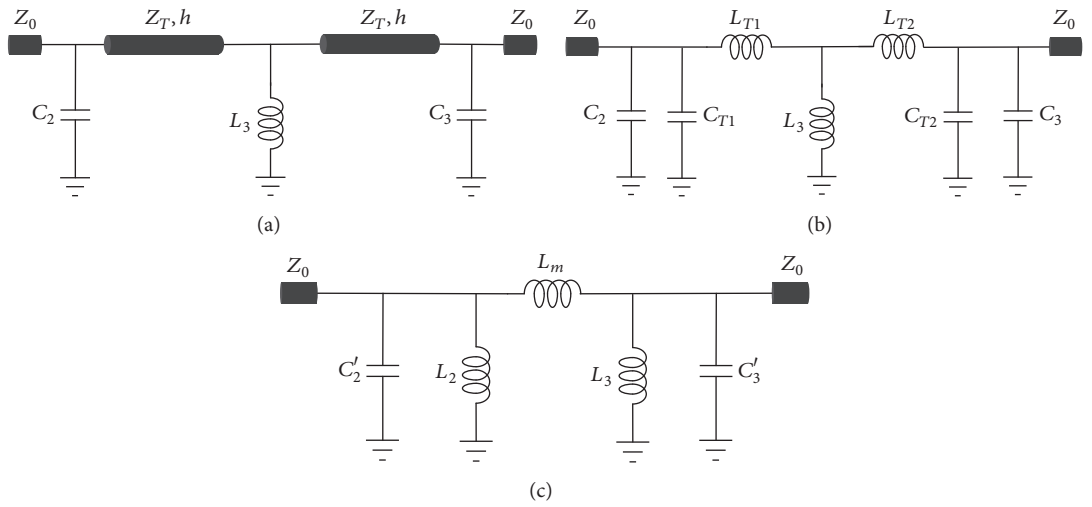

FIGURE 3: (a) The equivalent circuit model of high-frequency passband (b). The simplified circuit model of (a). (c) Simplified by converting the T-network to π-network.

desired response type provided in [30]. The equivalent inductance and capacitance of transmission lines are calculated by the following equations presented in [30]:

$$L_{Ti} = \mu_0 \mu_r h_i,$$
$$C_{Ti} = \frac{\varepsilon_0 \varepsilon_r h_i}{2}, \tag{3}$$

where $i = 1, 2$, h_i is the length of transmission line (the thickness of dielectric substrate), and ε_0 and μ_0 are permittivity and permeability in free space, while ε_r and μ_r are relative permittivity and permeability of the dielectric substrate. Subsequently, the capacitances are calculated as follows:

$$C_2 = \frac{q_1}{w_0 Z_0 r_1 \delta} - C_{T1}, \tag{4a}$$
$$C_3 = \frac{q_2}{w_0 Z_0 r_2 \delta} - C_{T2}. \tag{4b}$$

Based on the formulas mentioned above, the parameters in Figure 2 can be obtained. In summary, the synthesis procedure of the proposed dual-band FSS can be simplified as follows.

(1) With the given center frequency f_{02}, fractional bandwidth δ, and the response type, inductors L_{T1}, L_{T2}, and L_s can be calculated using (2).

(2) Then we can obtain C_2 and C_3 using (3)–(4b).

(3) Based on the given transmission zero and poles (f_{z1} and f_{01}), we can calculate L_1 and C_1 using (1).

The next step is to map the equivalent parameters in Figure 2 to the geometric parameters of the dual-band FSS in Figure 1. The initial values of dimensions of the unit cell can be calculated using the formulas in [29, 31–33]. The following equations give the relations between geometrical parameters of the dual-band FSS and circuit parameters.

$$\frac{X_{L1}}{Z_0} = wL_1 = \frac{L_0}{D} \cos\theta F\left(D, 2w_0, \lambda, \theta\right), \tag{5a}$$
$$\frac{X_{Ls}}{Z_0} = wL_s = \frac{D - L_0}{D} \cos\theta F\left(D, 2s_1, \lambda, \theta\right), \tag{5b}$$
$$\frac{B_{C_1}}{Y_0} = wC_1 = 4\frac{l}{D} \sec\theta F\left(D, w, \lambda, \theta\right) \varepsilon_{\text{eff}}, \tag{5c}$$
$$\frac{B_{C_2}}{Y_0} = wC_2 = 4\frac{L}{D} \sec\theta F\left(D, s, \lambda, \theta\right) \varepsilon_{\text{eff}}, \tag{5d}$$

where λ represents the operating wavelength of each passband, θ is the incident angle, and l is the total length of the convoluted cross dipole aperture in the middle layer. The factor $\varepsilon_{\text{eff}} = 0.5(\varepsilon_r + 1)$ is the effective dielectric permittivity. Factor F stands for the normalized inductance or capacitance of the strip grating which has been summarized in [31]

$$F\left(D, w, \lambda, \theta\right) = \frac{D}{\lambda}\left[\ln\csc\left(\frac{\pi w}{2D}\right) + G\left(D, w, \lambda, \theta\right)\right], \tag{6}$$

where G is the correction term. It is important to note that the values calculated from (1) to (6) are approximate values. These values are used as the initial values to tune the dimensions using CST-MWS to obtain the desired filtering response.

3. Simulation and Experimental Verification

3.1. Simulation Results. The center frequencies are selected, respectively, $f_{01} = 2.82$ GHz, $f_{z1} = 4.17$ GHz, and $f_{02} = 7.82$ GHz, with the fractional bandwidth of the high-frequency band being $\delta = 30\%$. For the Butterworth response, the values are $q_1 = q_2 = 1.4142$ $k_{12} = 0.70711$ and $r_1 = r_2 = 1$. The dielectric substrate is RO4350B with $\varepsilon_r = 3.5$ and $\mu_r = 1$. The desired equivalent circuit parameters of the dual-band FSS are calculated using (1)–(6) where $L_1 = 429.24$ pH, $L_s = 361.73$ pH, and $C_2 = C_3 = 238.04$ fF. These values are used to compute the frequency response of the dual-band FSS by the circuit simulation software ADS. The thickness of the material is 1.06 mm, which is not commercially available. The thickness has been changed to 0.762 mm, which is the closest commercially available thickness used for

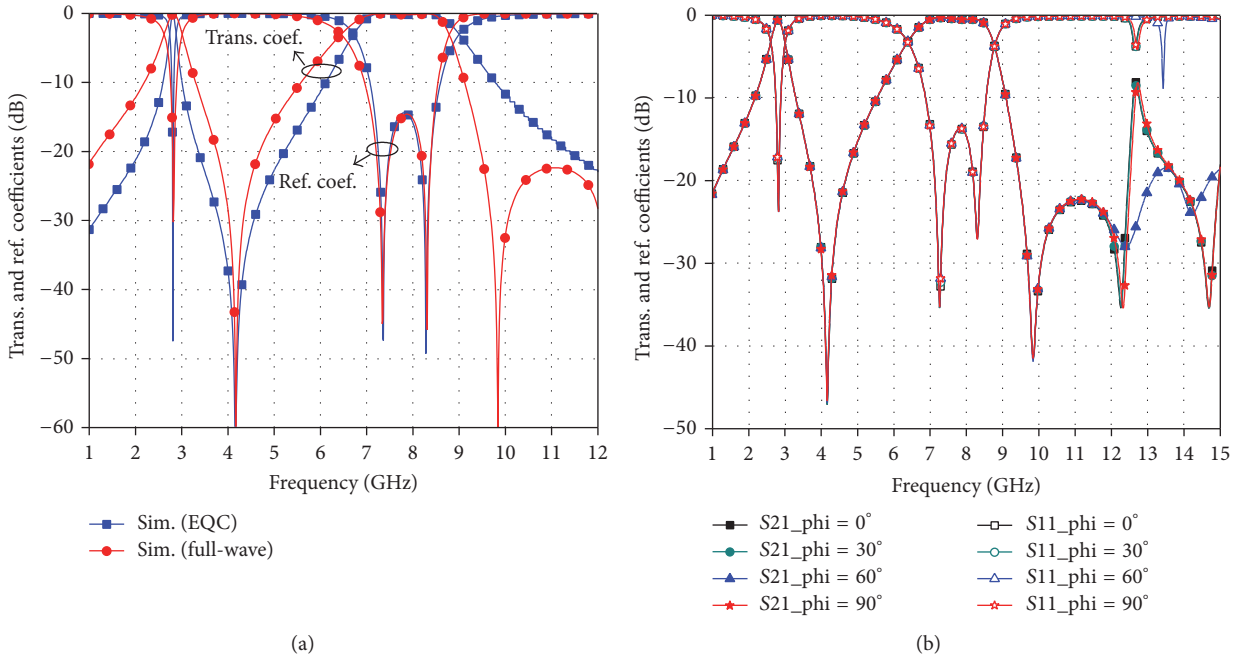

FIGURE 4: (a) Comparison of transmission and reflection coefficients of the dual-band FSS calculated by CST and the equivalent circuit. (b) Transmission coefficients of the FSS under different polarization.

the substrate. The values of circuit elements must be tuned in order to regain the desired filter response. The optimized values of the circuit parameters as well as the optimized geometric parameters using CST-MWS are listed in Table 1.

Figure 4(a) shows the transmission and reflection coefficients of the dual-band FSS simulated in CST alongside the frequency response calculated by the equivalent circuit model in Figure 2. A decent agreement between the two results is observed. It is seen that a dual-band response around f_{01} = 2.82 GHz and f_{02} = 7.82 GHz has been achieved. A transmission zero f_{z1} = 4.17 GHz is obtained, which improves the selectivity of the proposed FSS. As observed, the bandwidth calculated by ADS is narrower than that calculated by CST, which is attributed to the effect of the dielectric substrate. The coupling effect between the square metal patches and the middle metal layer produces a transmission zero at 9.89 GHz. The influence is ignored in circuit analysis. The FSS response is affected by not only its geometry but also the incident angle and the polarization of EM wave. Figure 4(b) shows the response that stays stable under different polarization and exhibits wide out-of-band rejection. The unit size is $0.089\lambda \times 0.089\lambda$ and the thickness is 0.014λ. Compared with the multilayer FSSs and 3D FSSs presented in previous works, the proposed FSS exhibits smaller element size and lower profile. It also achieves a good performance of angular stability. The comparison results are listed in Table 2.

Figure 5 shows the results of transmission coefficients, which are relatively stable for TE and TM polarization when the incident angle is changing from 0° to 60°. There is no modal interaction null in the high-frequency band. As observed, for TE polarization, the bandwidth decreases with the increase of the incident angle, while the TM polarization is the opposite. The observed changes can be illustrated by the variation of wave impedance [38]. In the case of TE polarization, the wave impedance ($Z_{TE} = Z_0/\cos\theta$) increases with the increase of the incident angle, and then the quality factor of the filter's resonator decreases, which causes the reduction of the bandwidth of resonator. For TM polarization, the wave impedance ($Z_{TM} = Z_0 \cos\theta$) decreases with the increase of the incident angle, which causes the decreasing of the quality factor of filter's resonator, and the bandwidth of the FSS is broadened.

3.2. Controllable Mechanism. The geometry parameters of the dual-band FSS directly affect the characteristics of transmission. Figure 6 shows the results of the dual-band FSS with respect to different lengths of the slots. The transmission zero shifts to a lower frequency when the length increases. When L_0 = 0 mm, the structure has no slots as shown in Figure 6. In this case, there is no transmission zero between the two passbands. The transmission zero f_{z1} reduces from 5.66 GHz to 4.07 GHz when L_0 increased from 4.8 mm to 7.2 mm. It can be concluded that etching slots are effective in improving the characteristics of frequency selectivity and miniaturization.

A polarization selective surface is going to be obtained when the length of slots in horizontal and vertical directions is different, as shown in Figure 7. For TE polarization, there is a transmission zero between the two passbands when slots are etched horizontally, while there is no transmission zero for TM polarization and vice versa.

Figure 8 shows the transmission characteristics of the dual-band FSS with respect to different lengths of patches. The high-frequency band will shift to a lower frequency when the length L increased. In the circuit model, C_2 and C_3 are

Table 2: Results comparison to other multilayered and 3D FSS structures.

ε_r	Ref.	Unit cell dimension	Thickness	Max. of incidence angle
2.65	[16]	$0.18\lambda \times 0.18\lambda$	0.05λ	60°
	[34]	$0.23\lambda \times 0.23\lambda$	0.11λ	50°
	[35]	$0.12\lambda \times 0.12\lambda$	0.008λ	45°
	[36]	$0.1\lambda \times 0.1\lambda$	0.033λ	60°
	This FSS	$0.104\lambda \times 0.104\lambda$	0.017λ	60°
3	[25]	$0.3\lambda \times 0.3\lambda$	0.217λ	40°
	This FSS	$0.098\lambda \times 0.098\lambda$	0.016λ	60°
3.4	[37]	$0.17\lambda \times 0.17\lambda$	0.033λ	45°
	This FSS	$0.092\lambda \times 0.092\lambda$	0.015λ	60°
3.5	[38]	$0.125\lambda \times 0.125\lambda$	0.0062λ	45°
	This FSS	$0.089\lambda \times 0.089\lambda$	0.014λ	60°
3.55	[22]	$0.1\lambda \times 0.08\lambda$	0.09λ	45°
	This FSS	$0.09\lambda \times 0.09\lambda$	0.014λ	60°
10.7	[19]	$0.105\lambda \times 0.105\lambda$	0.039λ	45°
	This FSS	$0.054\lambda \times 0.054\lambda$	0.009λ	60°

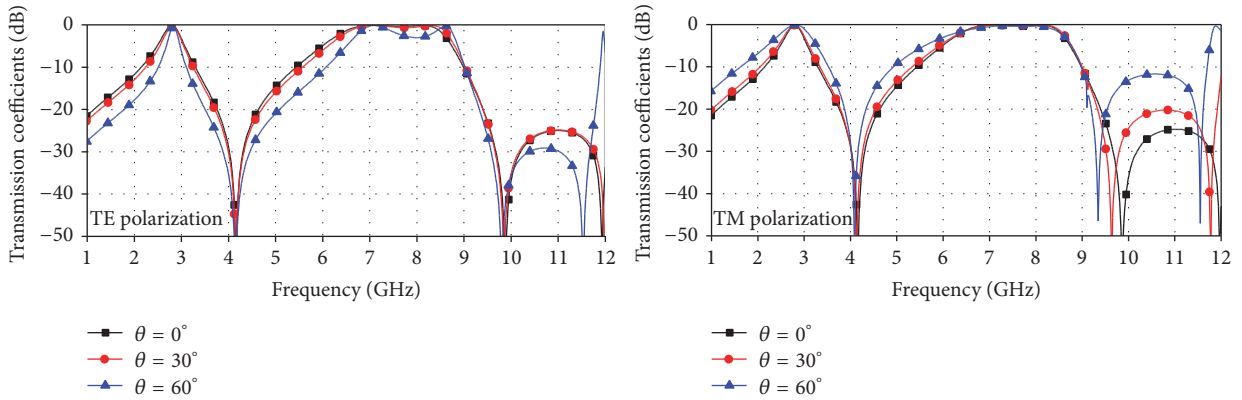

Figure 5: Transmission coefficients of the dual-band FSS under different incident angles.

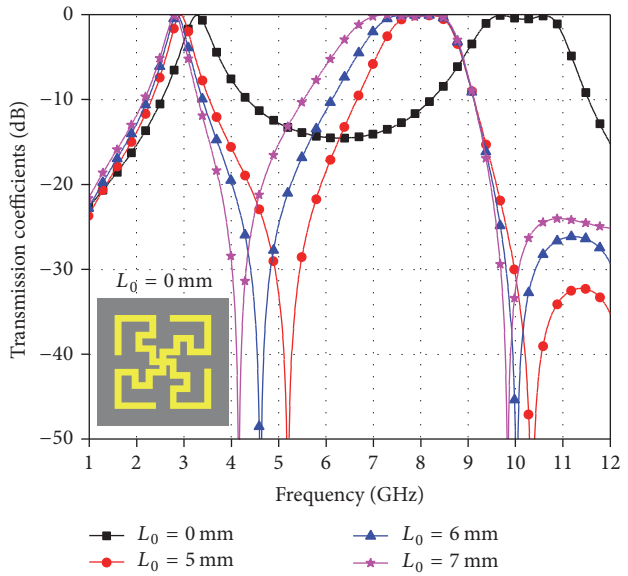

Figure 6: Transmission coefficients of the dual-band FSS with the different length of slots.

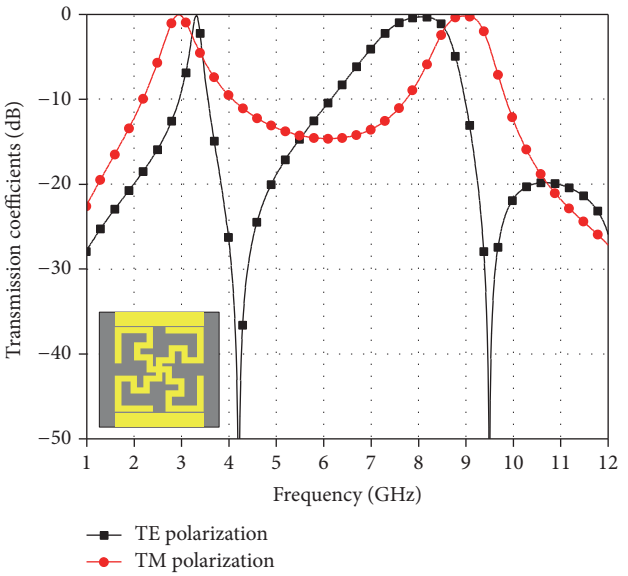

Figure 7: Transmission coefficients of the dual-band FSS with the slots etching in horizontal direction.

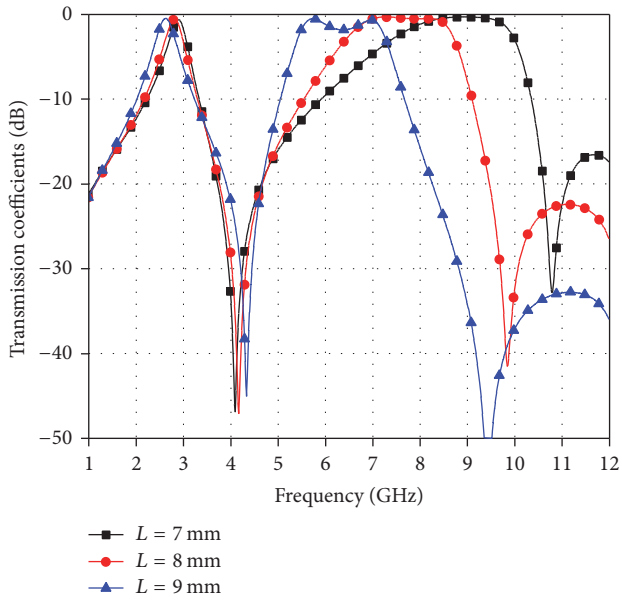

Figure 8: Transmission coefficients of the dual-band FSS with the different size of the patches.

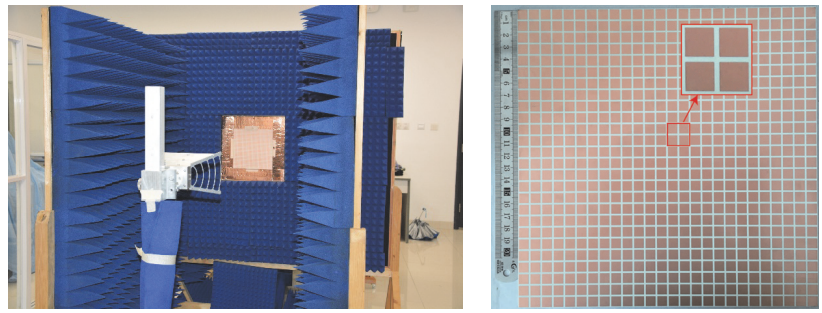

(a) (b)

Figure 9: (a) Photograph of the measurement setup. (b) Photograph of the fabricated FSS.

proportional to the length L and are inversely proportional to the gap s. Therefore, the resonant frequency f_{02} has reduced from 8.75 GHz to 6.35 GHz when the length L increased from 7 mm to 9 mm.

3.3. Experimental Results. The performance of the high selectivity dual-band FSS is experimentally verified by fabricating a prototype with 26 × 26 elements and measuring the frequency response using a free space measurement setup. The size of the prototype is 247 mm × 247 mm. The thickness of the RO4350B substrate is 0.762 mm. The two substrates are thermally compressed together with a bonding film (S7116) with a thickness of 0.127 mm in between them. Figure 9 shows the photographs of FSS and the measurement setup. Figure 10 compares the measured results of the dual-band FSS and the simulation results. As observed, the FSS has two passbands around 2.82 GHz and 7.82 GHz and the simulation results agree with the measurement results fairly well. Furthermore, the frequency response of the dual-band FSS at different incident angles is also examined as shown in Figure 11.

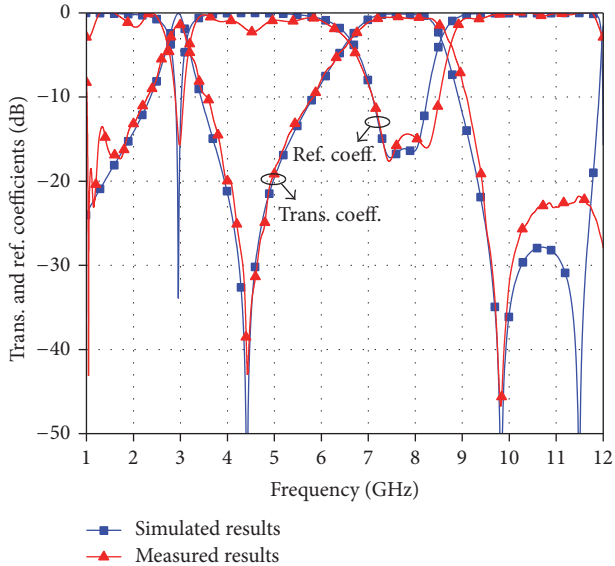

Figure 10: Simulated and measured results of fabricated FSS.

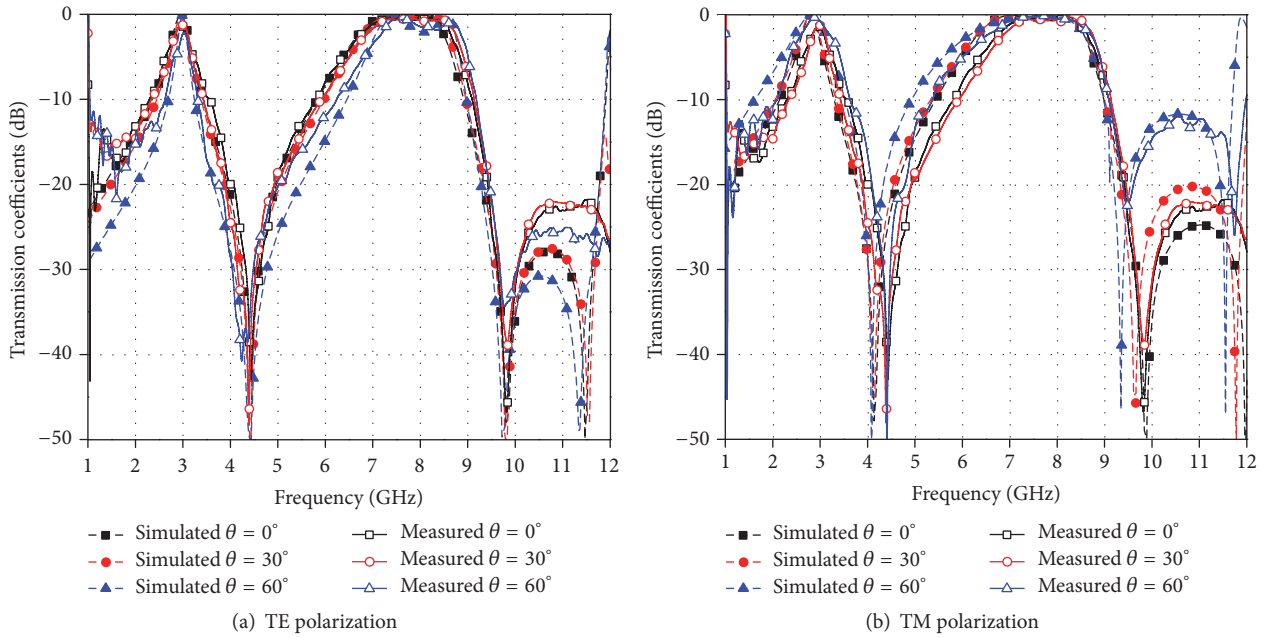

Figure 11: Measured and simulated transmission coefficients of the dual-band FSS for oblique incident angles from 0° to 60°. (a) TE polarization. (b) TM polarization.

The frequency response is relatively stable for both TE and TM polarization for incident angles within the range of 0–60 degrees. The discrepancy between the simulated and measured results is mainly attributed to the effect of bonding film. It also increases the insertion loss in all operating bands.

4. Conclusions

In this paper, a novel, highly selective, low profile, dual-band frequency selective surface with a controllable transmission zero is proposed, and the transmission zero is introduced by etching slots on the middle layer. A frequency selective surface with a controllable transmission zero and polarization selectivity is able to be obtained from tuning the size and locating the direction of the slots. The design procedure based on the equivalent circuit model is presented. The dual-band FSS is analyzed, fabricated, and measured for a demonstration. The results show that the FSS has two passbands which exhibit outstanding performance of high selectivity, angular stability, and wide out-of-band rejection. Compared with the multilayered dual-band FSSs proposed in previous works, the proposed FSS with a controllable transmission zero has the advantage of low profile and miniaturization. It shows excellent comprehensive performance and application prospect.

Conflicts of Interest

The authors declare that there are no conflicts of interest regarding the publication of this paper.

Acknowledgments

This paper was supported by National Defense "973" Basic Research Development Program of China (no. 6131380101). This paper was also supported by Pre-Research Fund of the 12th Five-Year Plan (no. 4010403020102 and no. 4010103020103) and the Fundamental Research Funds for the Central Universities (nos. HEUCFD1433 and HEUCF1508).

References

[1] B. A. Munk, *Frequency Selective Surfaces: Theory and Design*, vol. 319, A Wiley-lnterscience Publication, NY, USA, 2000.

[2] Q. Chen and Y. Fu, "A planar stealthy antenna radome using absorptive frequency selective surface," *Microwave and Optical Technology Letters*, vol. 56, no. 8, pp. 1788–1792, 2014.

[3] M. Zahir Joozdani, M. Khalaj Amirhosseini, and A. Abdolali, "Wideband radar cross-section reduction of patch array antenna with miniaturised hexagonal loop frequency selective surface," *Electronics Letters*, vol. 52, no. 9, pp. 767-768, 2016.

[4] A. Edalati and K. Sarabandi, "Reflectarray antenna based on grounded loop-wire miniaturised-element frequency selective surfaces," *IET Microwaves, Antennas and Propagation*, vol. 8, no. 12, pp. 973–979, 2014.

[5] A. Chatterjee and S. K. Parui, "Performance enhancement of a dual-band monopole antenna by using a frequency-selective surface-based corner reflector," *Institute of Electrical and Electronics Engineers. Transactions on Antennas and Propagation*, vol. 64, no. 6, pp. 2165–2171, 2016.

[6] E. Moharamzadeh, "Radiation characteristic improvement of X-band slot antenna using new multiband frequency-selective surface," *International Journal of Antennas and Propagation*, vol. 2014, Article ID 321287, 9 pages, 2014.

[7] D. Gangwar, S. Das, R. L. Yadava, and B. K. Kanaujia, "Circularly polarized inverted stacked high gain antenna with frequency selective surface," *Microwave and Optical Technology Letters*, vol. 58, no. 3, pp. 732–740, 2016.

[8] H. Wang, P. Kong, W. Cheng et al., "Broadband tunability of polarization-insensitive absorber based on frequency selective surface," *Scientific Reports*, vol. 6, Article ID 23081, 2016.

[9] Q. Zhang, L. Bai, X. Liu, C. Liu, and X. Cui, "Simplified transparent conductive oxides-based ultrabroadband absorber design," *Journal of Lightwave Technology*, vol. 34, no. 4, Article ID 7374650, pp. 1354–1359, 2016.

[10] W. Li, C. Wang, Y. Zhang, and Y. Li, "A miniaturized frequency selective surface based on square loop aperture element," *International Journal of Antennas and Propagation*, vol. 2014, Article ID 701279, 6 pages, 2014.

[11] R. A. Hill and B. A. Munk, "The effect of perturbating a frequency-selective surface and its relation to the design of a dual-band surface," *IEEE Transactions on Antennas and Propagation*, vol. 44, no. 3, pp. 368–374, 1996.

[12] S. Ghosh and K. V. Srivastava, "An angularly stable dual-band FSS with closely spaced resonances using miniaturized unit cell," *IEEE Microwave and Wireless Components Letters*, vol. 27, no. 3, pp. 218–220, 2017.

[13] T. K. Wu, "Superior dual band FSS with fractal elements," in *Proceedings of the Radio Science Meeting (Joint with AP-S Symposium), 2014 USNC-URSI*, p. 152, IEEE, TN, USA, July 2014.

[14] D. Wang, W. Che, Y. Chang, K.-S. Chin, and Y.-L. Chow, "Combined-element frequency selective surfaces with multiple transmission poles and zeros," *IET Microwaves, Antennas and Propagation*, vol. 8, no. 3, pp. 186–193, 2014.

[15] X.-D. Hu, X.-L. Zhou, L.-S. Wu, L. Zhou, and W.-Y. Yin, "A miniaturized dual-band frequency selective surface (FSS) with closed loop and its complementary pattern," *IEEE Antennas and Wireless Propagation Letters*, vol. 8, pp. 1374–1377, 2009.

[16] M. Yan, J. Wang, H. Ma et al., "A tri-band, highly selective, bandpass FSS using cascaded multilayer loop arrays," *IEEE Transactions on Antennas and Propagation*, vol. 64, no. 5, pp. 2046–2049, 2016.

[17] H. Zhou, S.-B. Qu, B.-Q. Lin et al., "Dual band frequency selective surface based on circular aperture-coupled patches," *Microwave and Optical Technology Letters*, vol. 53, no. 8, pp. 1784–1786, 2011.

[18] M. A. Al-Joumayly and N. Behdad, "A generalized method for synthesizing low-profile, band-pass frequency selective surfaces with non-resonant constituting elements," *IEEE Transactions on Antennas and Propagation*, vol. 58, no. 12, pp. 4033–4041, 2010.

[19] M. Gao, S. M. Momeni Hasan Abadi, and N. Behdad, "A dual-band, inductively coupled miniaturized-element frequency selective surface with higher order bandpass response," *Institute of Electrical and Electronics Engineers. Transactions on Antennas and Propagation*, vol. 64, no. 8, pp. 3729–3734, 2016.

[20] M. Yan, J. Wang, S. Qu et al., "Highly-selective, closely-spaced, dual-band FSS with second-order characteristic," *IET Microwaves, Antennas and Propagation*, vol. 10, no. 10, pp. 1087–1091, 2016.

[21] S. Unaldi, S. Cimen, G. Cakir, and U. E. Ayten, "A novel dual-band ultrathin FSS with closely settled frequency response," *IEEE Antennas and Wireless Propagation Letters*, vol. 16, pp. 1381–1384, 2017.

[22] K. Tao, B. Li, Y. Tang, and Q. Wu, "Multi-layer tri-band frequency selective surface using stepped- and uniformimpedance resonators," *Electronics Letters*, vol. 52, no. 8, pp. 583–585, 2016.

[23] B. Li and Z. Shen, "Dual-band bandpass frequency-selective structures with arbitrary band ratios," *Institute of Electrical and Electronics Engineers. Transactions on Antennas and Propagation*, vol. 62, no. 11, pp. 5504–5512, 2014.

[24] A. A. Omar and Z. Shen, "Multiband high-order bandstop 3-D frequency-selective structures," *Institute of Electrical and Electronics Engineers. Transactions on Antennas and Propagation*, vol. 64, no. 6, pp. 2217–2226, 2016.

[25] B. Li and Z. Shen, "Synthesis of quasi-elliptic bandpass frequency-selective surface using cascaded loop arrays," *IEEE Transactions on Antennas and Propagation*, vol. 61, no. 6, pp. 3053–3059, 2013.

[26] B. Li and Z. Shen, "Three-dimensional bandpass frequency-selective structures with multiple transmission zeros," *IEEE Transactions on Microwave Theory and Techniques*, vol. 61, no. 10, pp. 3578–3589, 2013.

[27] Z. Bai, Q. Zhang, Y. Ju et al., "Flexible metamaterial narrow-band-pass filter based on magnetic resonance coupling between ultra-thin bilayer frequency selective surfaces," *Journal of Physics D: Applied Physics*, vol. 49, no. 6, Article ID 065002, 2015.

[28] J.-S. G. Hong and M. J. Lancaster, *Microstrip Filters for RF/Microwave Applications*, vol. 167, John Wiley Sons, 2004.

[29] Z. L. Wang, K. Hashimoto, N. Shinohara, and H. Matsumoto, "Frequency-selective surface for microwave power transmission," *IEEE Transactions on Microwave Theory and Techniques*, vol. 47, no. 10, pp. 2039–2042, 1999.

[30] G. L. Matthaei, L. Young, and E. M. Jones, *Design of Microwave Filters, Impedance-Matching Networks, and Coupling Structures. Volume 2*, DTIC Document, 1963.

[31] C. K. Lee and R. J. Langley, "Equivalent-circuit models for frequency-selective surfaces at oblique angles of incidence," *IEE Proceedings H - Microwaves, Antennas and Propagation*, vol. 132, no. 6, pp. 395–399, 1985.

[32] G. H.-H. Sung, K. W. Sowerby, M. J. Neve, and A. G. Williamson, "A frequency-selective wall for interference reduction in wireless indoor environments," *IEEE Antennas and Propagation Magazine*, vol. 48, no. 5, pp. 29–37, 2006.

[33] D. Ferreira, R. F. Caldeirinha, I. Cuiñas, and T. R. Fernandes, "Square loop and slot frequency selective surfaces study for equivalent circuit model optimization," *Institute of Electrical and Electronics Engineers. Transactions on Antennas and Propagation*, vol. 63, no. 9, pp. 3947–3955, 2015.

[34] X. Song, Z. Yan, T. Zhang, C. Yang, and R. Lian, "Triband Frequency-Selective Surface as Subreflector in Ku-, K-, and Ka-Bands," *IEEE Antennas and Wireless Propagation Letters*, vol. 15, pp. 1869–1872, 2016.

[35] H. Li and Q. Cao, "Design and analysis of a controllable miniaturized triband frequency selective surface," *Progress in Electromagnetics Research Letters*, vol. 52, pp. 105–112, 2015.

[36] M. Yan, S. Qu, J. Wang et al., "A miniaturized dual-band FSS with second-order response and large band separation," *IEEE Antennas and Wireless Propagation Letters*, vol. 14, pp. 1602–1605, 2015.

[37] M. Salehi and N. Behdad, "A second-order dual X-/Ka-band frequency selective surface," *IEEE Microwave and Wireless Components Letters*, vol. 18, no. 12, pp. 785–787, 2008.

[38] M. A. Al-Joumayly and N. Behdad, "Low-profile, highly-selective, dual-band frequency selective surfaces with closely spaced bands of operation," *IEEE Transactions on Antennas and Propagation*, vol. 58, no. 12, pp. 4042–4050, 2010.